

## Critical Star-Formation Rates for Reionization: Full Reionization Occurs at Redshift $z \approx 7$

J. Michael Shull, Anthony Harness, Michele Trenti

*CASA, Department of Astrophysical & Planetary Sciences,  
University of Colorado, Boulder, CO 80309*

Britton D. Smith, *Dept. of Physics & Astronomy, Michigan State University*

michael.shull@colorado.edu, trenti@colorado.edu,  
anthony.harness@colorado.edu, smit1685@msu.edu

### ABSTRACT

We assess the probable redshift ( $z_{\text{rei}} \approx 7$ ) for full reionization of the intergalactic medium (IGM) using a prescription for the co-moving star-formation-rate (SFR) density ( $\dot{\rho}_{\text{SFR}}$ ) required to maintain photoionization against recombination. Our newly developed on-line reionization simulator allows users to assess the required SFR and ionization histories, using a variety of assumptions for galactic and stellar populations, IGM clumping factor and temperature, and LyC escape fraction. The decline in high-redshift galaxy candidates and Ly $\alpha$  emitters at  $z = 6 - 8$  suggests a rising neutral fraction, with reionization at  $z \gtrsim 7$  increasingly difficult owing to increased recombination rates and constraints from the ionizing background and LyC mean free path. The required rate is  $\dot{\rho}_{\text{SFR}} \approx (0.018 M_{\odot} \text{ yr}^{-1} \text{ Mpc}^{-3})[(1+z)/8]^3 (C_H/3)(0.2/f_{\text{esc}})T_4^{-0.845}$  scaled to fiducial values of clumping factor  $C_H = 3$ , escape fraction  $f_{\text{esc}} = 0.2$ , electron temperature  $T_e = 10^4$  K, and low-metallicity initial mass functions (IMF) and stellar atmospheres. Our hydrodynamical + N-body simulations find a mean clumping factor  $C_H \approx (2.9)[(1+z)/6]^{-1.1}$  in the photoionized, photoheated filaments at  $z = 5 - 9$ . The critical SFR could be reduced by increasing the minimum stellar mass, invoking a top-heavy IMF, or systematically increasing  $f_{\text{esc}}$  at high  $z$ . The CMB optical depth,  $\tau_e = 0.088 \pm 0.015$ , could be explained by full reionization, producing  $\tau_e = 0.050$  back to  $z_{\text{rei}} \approx 7$ , augmented by  $\Delta\tau_e \approx 0.01 - 0.04$  in a partially ionized IGM at  $z > 7$ . In this scenario, the strongest 21-cm signal should occur at redshifted frequencies 124 – 167 MHz owing to IGM heating over an interval  $\Delta z \approx 3$  from  $z \approx 7.5 - 10.5$ .

*Subject headings:* Galaxies: high-redshift — intergalactic medium — reionization

## 1. INTRODUCTION

Our current hypothesis is that the galaxies and black holes observed today originated over 13 Gyr ago, growing from seeds of primordial density perturbations. One can test this hypothesis by studying the star formation rate (SFR) history, from the Epoch of Reionization (EoR) at redshifts  $6 < z < 12$ , through the peak era at  $z \approx 2 - 3$  (Hopkins & Beacom 2006) down to the present epoch. The feedback of ionizing radiation, kinetic energy, and heavy elements leaves imprints on early stars, supernovae, and galaxies, providing a “fossil record” that can be detected through abundances in Galactic halo stars and the intergalactic medium (IGM) and in the distributions of mass, metallicity, and luminosity of galaxies.

Determining when and how the universe was reionized by these early sources have been important questions for decades (Gunn & Peterson 1965; Sunyaev 1977; Robertson et al. 2010). It has been suggested that IGM reionization was complete by  $z \approx 6.5$  (Fan et al. 2001; Gnedin & Fan 2006; Fan et al. 2006; Hu & Cowie 2006), based on strong Ly $\alpha$  absorption from neutral hydrogen along lines of sight to QSOs at  $z > 6$ . Becker et al. (2007) and Songaila (2004) used transmission of the Ly $\alpha$  (and Ly $\beta$ ) forest out to  $z = 5.8$  and  $z = 6.3$ , respectively, to suggest a smoothly decreasing ionization rate toward higher redshifts. Recent surveys of high-redshift galaxies and Ly $\alpha$  emitters (Bouwens et al. 2011a; Ouchi et al. 2010; Kashikawa et al. 2011; Ono et al. 2012; Schenker et al. 2012) infer an increasing IGM neutral fraction from the declining populations between  $z = 6 - 8$ . Further evidence for an increasing neutral fraction comes from the decreasing sizes of ionized “near zones” associated with quasars between  $z = 5.7$  and  $z = 6.4$  (Carilli et al. 2010) and from the Ly $\alpha$  damping wing in the transmission profile toward the newly discovered quasar at  $z = 7.085$  (Mortlock et al. 2011). These studies all suggest that the IGM is becoming increasingly neutral between  $z = 6 - 7$ , marking the end of cosmic reionization when ionized regions overlap and percolate. Whether the epoch of full reionization occurs at  $z_{\text{rei}} \approx 7$  is still not ascertained.

A contrasting estimate of the EoR comes from the measured optical depth,  $\tau_e = 0.088 \pm 0.015$ , to electron scattering of the cosmic microwave background (CMB) in *WMAP-7* observations (Larson et al. 2011; Komatsu et al. 2011). The error bars come from the central 68% in the marginalized cumulative distribution. Using additional cosmological parameter constraints, they infer single-epoch reionization at  $z_{\text{rei}} = 10.6 \pm 1.2$ . Although such a high redshift could be explained with  $\Lambda$ CDM simulations and modeled SFR histories (Choudhury & Ferrara 2005; Trac & Cen 2007; Shull & Venkatesan 2008), the CMB observations are at variance with optical surveys that suggest late reionization, unless reionization is a process

that extends to higher redshifts.

For a fully ionized IGM, including both H and He, the optical depth  $\tau_e = 0.050$  for  $z_{\text{rei}} = 7.0$  (see Section 2.1). In the CMB analysis (Larson et al. 2011), marginalization of  $\tau_e$  with other cosmological parameters allows the possibility of lower optical depth, with a reionization epoch as low as  $z_{\text{rei}} \sim 7 - 8$  at 95% C.L. One can also invoke a partially ionized IGM at  $z_{\text{rei}} > 7$ , as discussed by many groups (Cen 2003; Venkatesan et al. 2003; Ricotti & Ostriker 2004; Benson et al. 2006; Shull & Venkatesan 2008). However, even with the recent progress in finding high- $z$  galaxies, we still do not know whether galaxies are the sole agents of reionization. Current observations of high- $z$  galaxies leave open several ionization scenarios, some involving simple hydrogen reionization at  $z \approx 10$  and He II reionization at  $z \approx 3$ , and others with more complex ionization histories (Bolton & Haehnelt 2007; Venkatesan, Tumlinson & Shull 2003; Cen 2003) that depend on SFRs at  $z = 7 - 20$ . Shull & Venkatesan (2008) demonstrated how the CMB optical depth constrains the SFR and IGM metallicity history at  $z > 7$ , and Trenti & Shull (2010) quantified the metallicity-driven transition from Population III (metal-free stars) to Population II (stars formed from metal-enriched gas).

Several recent observations provide valuable constraints on the luminosity function of high- $z$  galaxies. The number density of galaxies appears to drop rapidly at  $z > 7$  (Bouwens et al. 2009, 2010a,b, 2011a,b,c). With a comoving SFR density  $\dot{\rho}_* \lesssim 0.01 M_\odot \text{ yr}^{-1} \text{ Mpc}^{-3}$  at  $z \approx 7$  (González et al. 2010; Bouwens et al. 2011a), the observed galaxies do not produce enough ionizing photons in the Lyman continuum (LyC) to maintain a photoionized IGM against recombinations. However, the luminosity function is steep, and the total LyC budget requires extrapolation to low-luminosity galaxies (Trenti et al. 2010; Bouwens et al. 2011b). Moreover, the conversion from SFR to LyC production rate relies on insecure calibrations from theoretical models and comparison with high-mass, low-metallicity stars. We revisit the calculation of LyC photon production and assess the high- $z$  galaxy contribution to reionization. We also analyze several factors, such as the photon escape fraction ( $f_{\text{esc}}$ ), IGM clumping factor ( $C_H$ ), and electron temperature ( $T_e$ ), which enter the calculation of the “critical star formation rate” ( $\dot{\rho}_{\text{crit}}$ ) necessary to maintain a photoionized IGM.

In Section 2, we calculate  $\dot{\rho}_{\text{crit}}$  ( $M_\odot \text{ yr}^{-1} \text{ Mpc}^{-3}$ ) in a filamentary IGM, equating the production rate of Lyman continuum (LyC) photons with the hydrogen recombination rate. The photoionization rate depends on the mass function of stellar populations, their evolutionary tracks and stellar atmospheres, and the escape fraction,  $f_{\text{esc}}$  of LyC photons away from their galactic sources. The recombination rate depends on the density and temperature of the IGM, properties we explore with cosmological simulations. In Section 3, we give our results for the critical SFR at  $z \gtrsim 6$  and present our new SFR simulator, a user-friendly interface for calculating  $\dot{\rho}_{\text{crit}}(z)$  and  $\tau_e(z)$ . In Section 4, we discuss the implications for the

hydrogen EoR. Consistency between high-redshift galaxies and CMB optical depth appears to require  $z_{\text{rei}} \approx 7$  and a partially ionized IGM at  $z > 7$ . The peak signal from redshifted 21-cm emission would likely occur during the heating period between  $z = 7.7 - 8.8$  (145–163 MHz) when the hydrogen neutral fraction  $x_{\text{HI}} \approx 0.5$  (Pritchard et al. 2010; Lidz et al. 2008).

## 2. REIONIZATION WITH CLUMPING AND PHOTON ESCAPE

### 2.1. Reionization and Critical Star Formation Rate

We denote by  $\dot{\rho}_{\text{SFR}}$  ( $M_{\odot} \text{ yr}^{-1} \text{ Mpc}^{-3}$ ) the global star formation rate per co-moving volume. Using a simple argument (Madau et al. 1999), balancing photoionization with radiative recombination, we estimate the critical SFR to maintain IGM photoionization at  $z > 7$ , assuming that the LyC photons are produced by populations of massive (OB-type) stars. Because the mass in collapsed objects (clusters, groups, galaxies) is still small at high redshift, the IGM contains most of the cosmological baryons, at mean density

$$\bar{\rho}_b = \Omega_b \rho_{\text{cr}} (1+z)^3 = (4.24 \times 10^{-31} \text{ g cm}^{-3}) (1+z)^3. \quad (1)$$

For a Hubble constant denoted  $H_0 = (100 \text{ km s}^{-1} \text{ Mpc}^{-1}) h$ , we adopt the WMAP-7 (plus BAO +  $H_0$ ) parameters,  $\Omega_b h^2 = 0.02255 \pm 0.00054$  and  $\Omega_m h^2 = 0.1352 \pm 0.0036$  (Komatsu et al. 2011) relative to a critical density  $\rho_{\text{cr}} = 1.8785 \times 10^{-29} h^2 \text{ g cm}^{-3}$ . From the corresponding helium mass fraction  $Y = 0.2477 \pm 0.0029$  (Peimbert et al. 2007), we adopt a mean hydrogen number density,

$$\bar{n}_H = \frac{\bar{\rho}_b (1-Y)}{m_H} = (1.905 \times 10^{-7} \text{ cm}^{-3}) (1+z)^3. \quad (2)$$

In a fully ionized IGM, the CMB optical depth back to  $z_{\text{rei}}$  can be written as the integral of  $n_e \sigma_T d\ell$ , the electron density times the Thomson cross section along proper length,

$$\tau_e(z_{\text{rei}}) = \int_0^{z_{\text{rei}}} n_e \sigma_T (1+z)^{-1} [c/H(z)] dz, \quad (3)$$

for a standard  $\Lambda$ CDM cosmology ( $\Omega_m + \Omega_{\Lambda} = 1$ ) with  $H(z) = H_0 [\Omega_m (1+z)^3 + \Omega_{\Lambda}]^{1/2}$ . This integral can be done analytically (Shull & Venkatesan 2008),

$$\tau_e(z_{\text{rei}}) = \left( \frac{c \sigma_T}{H_0} \right) \left( \frac{2\Omega_b}{3\Omega_m} \right) \left[ \frac{\rho_{\text{cr}} (1-Y)(1+y)}{m_H} \right] \left[ \{\Omega_m (1+z_{\text{rei}})^3 + \Omega_{\Lambda}\}^{1/2} - 1 \right]. \quad (4)$$

In the high-redshift limit, when  $\Omega_m (1+z)^3 \gg \Omega_{\Lambda}$ , this expression simplifies to

$$\tau_e(z_{\text{rei}}) \approx \left( \frac{c \sigma_T}{H_0} \right) \left( \frac{2\Omega_b}{3\Omega_m^{1/2}} \right) \left[ \frac{\rho_{\text{cr}} (1-Y)(1+y)}{m_H} \right] (1+z_{\text{rei}})^{3/2} \approx (0.0521) \left[ \frac{(1+z_{\text{rei}})}{8} \right]^{3/2} \quad (5)$$

independent of  $h$  to lowest order. The helium and electron densities are written  $n_{\text{He}} = yn_H$  and  $n_e = n_H(1+y)$  for singly ionized helium, where  $y = n_{\text{He}}/n_H = (Y/4)/(1-Y) \approx 0.0823$  by number. To these formulae, we add  $\Delta\tau_e \approx 0.002$ , from electrons donated by He III reionized at  $z \leq 3$  (Shull et al. 2010). Helium therefore contributes  $\sim 8\%$  to  $\tau_e$ , and a fully ionized IGM produces  $\tau_e = 0.050, 0.060,$  and  $0.070$  back to redshifts  $z_{\text{rei}} = 7, 8,$  and  $9,$  respectively.

A comoving volume of  $1 \text{ Mpc}^3$  contains  $N_H = 5.6 \times 10^{66}$  hydrogen atoms. Our simple ionization criterion requires a SFR density that produces a number of LyC photons equal to  $N_H$  over a hydrogen recombination time,  $t_{\text{rec}} = [n_e \alpha_H^{(B)} C_H]^{-1}$ . The hydrogen Case-B recombination rate coefficient (Osterbrock & Ferland 2006) is  $\alpha_H^{(B)}(T) \approx (2.59 \times 10^{-13} \text{ cm}^3 \text{ s}^{-1}) T_4^{-0.845}$ , scaled to an IGM temperature  $T = (10^4 \text{ K}) T_4$ . For typical IGM ionization histories and photoelectric heating rates, numerical simulations predict that diffuse photoionized filaments of hydrogen have temperatures ranging from 5000 K to 20,000 K (Davé et al. 2001; Smith et al. 2011). These are consistent with temperatures inferred from observations of the Ly $\alpha$  forest at  $z < 5$  (Becker et al. 2011).

Owing to gravitational instability, a realistic IGM is inhomogenous and filamentary. Semi-analytical models of the reionization of the universe often adopt a “clumping factor”,  $C_H \equiv \langle n_e^2 \rangle / \langle n_e \rangle^2$ , to account for inhomogeneity in estimates of the enhanced recombination rate in denser IGM filaments. The clumping factor therefore plays an important role in computing the critical SFR density needed to maintain the reionization of the universe. The clumping factor is also used in numerical simulations to implement “sub-grid physics”, in which changes in the density field occur on scales below the resolution of the simulation and are also approximated by the factor  $C_H$  (Gnedin & Ostriker 1997; Madau et al. 1999; Miralda-Escudé et al. 2000; Miralda-Escudé 2003; Kohler et al. 2007).

We correct the recombination time for density variations scaled to a fiducial  $C_H \approx 3$ , found in the simulations described below. At  $z \approx 7$ , the IGM filaments have electron density  $n_e \approx (10^{-4} \text{ cm}^{-3}) [(1+z)/8]^3 C_H$ , and the characteristic times for hydrogen recombination and Hubble expansion are,

$$t_{\text{rec}} \approx (386 \text{ Myr}) (3/C_H) T_4^{0.845} \left[ \frac{(1+z)}{8} \right]^{-3}, \quad (6)$$

$$t_H \approx [H_0 \Omega_m^{1/2} (1+z)^{3/2}]^{-1} \approx (1.18 \text{ Gyr}) \left[ \frac{(1+z)}{8} \right]^{-3/2}. \quad (7)$$

In our calculations, we express the reionization criterion as  $N_H (\text{Mpc}^{-3}) = \dot{\rho}_{\text{crit}} t_{\text{rec}} Q_{\text{LyC}} f_{\text{esc}}$ , where  $\dot{\rho}_{\text{crit}}$  is the critical SFR density ( $M_\odot \text{ yr}^{-1} \text{ Mpc}^{-3}$ ) and  $Q_{\text{LyC}}$  is the conversion factor from  $\dot{\rho}_{\text{SFR}}$  to the LyC production rate (see Section 2.2). We define  $f_{\text{esc}}$  as the fraction of LyC photons that escape from their galactic sources into the IGM (Dove & Shull 1994).

Recent statistical estimates (Nestor et al. 2011) suggest that  $f_{\text{esc}} \approx 0.1$  for an ensemble of 26 Lyman-break galaxies and 130 Ly $\alpha$  emitters at  $z \approx 3.09 \pm 0.03$ , and it could be higher for the lower-mass galaxies that likely dominate the escaping LyC at  $z > 6$  (Fernandez & Shull 2011). The LyC production efficiency,  $Q_{\text{LyC}}$ , is expressed in units  $10^{63}$  photons per  $M_{\odot}$  of star formation, since typical massive stars emit  $(1 - 10) \times 10^{63}$  LyC photons over their lifetime. To evaluate  $Q_{\text{LyC}}$ , we convert the SFR (by mass) into numbers of OB-stars and compute the total number of ionizing photons produced by a star of mass  $m$  over its lifetime. We then integrate over an IMF,  $\Psi(m) = Km^{-\alpha}$ , with a range  $m_{\text{min}} < m < m_{\text{max}}$ . The standard mass range is  $0.1 M_{\odot}$  to  $100 M_{\odot}$ , but changes in the mass range and IMF slope will affect the LyC production substantially. For example, differences in the IMF have been associated with higher Jeans masses in low-metallicity gas in the high-redshift IGM (Abel et al. 2002; Bromm & Loeb 2003), and Tumlinson (2007) and Smith et al. (2009) noted the potential influence of CMB temperature on modes of high-redshift star formation. Consequently, most cosmological simulations or calculations include a metallicity-induced IMF transition (Trenti & Shull 2010) between low-metallicity Population III star formation and metal-enhanced Population II.

## 2.2. Ionizing photon luminosities

The number of LyC photons produced per total mass in star formation depends on the IMF of the stellar population and is given by the conversion factor  $Q_{\text{LyC}}$ . We calculate this conversion by integrating the total number of LyC photons produced over the entire mass in star formation.

$$Q_{\text{LyC}} \equiv \frac{N_{\text{LyC}}}{\dot{\rho}_{\text{SFR}} t_{\text{rec}}} = \frac{\int_{m_{\text{OB}}}^{m_{\text{max}}} \Psi(m) Q(m) dm}{\int_{m_{\text{min}}}^{m_{\text{max}}} \Psi(m) m dm}. \quad (8)$$

Here,  $Q(m)$  is the lifetime-integrated number of LyC photons as a function of mass calculated from stellar atmosphere models and evolutionary tracks. The IMF,  $\Psi(m) = Km^{-\alpha}$ , is integrated over the mass range  $m_{\text{min}} < m < m_{\text{max}}$ , where  $m$  is expressed in solar units. In the SFR simulator discussed in Section 3.3, the user can choose between a normal and broken IMF power law. The lower integration limit in the numerator,  $m_{\text{OB}}$ , is the mass at which stars no longer produce significant amounts of LyC photons.

In our calculator, we use and compare two models that calculate  $Q(m)$ . First, using stellar atmospheres and evolutionary tracks (R. S. Sutherland & J. M. Shull, unpublished), we find that, over its main-sequence and post-main-sequence lifetime, an OB star of mass  $m$  produces a total number  $N_{\text{LyC}} = Q_{63}(m) \times 10^{63}$  of ionizing photons, where  $Q_{63} \approx 1 - 10$  over the mass range  $m = 30 - 100$  and for metallicities  $Z = (0.02 - 2.0)Z_{\odot}$ . We have fitted



our results to the form  $Q_{63}(m) \approx Am - B$ , for  $m \geq m_{\text{OB}} = B/A$  (the mass  $m_{\text{OB}}$  defines the effective lower limit for stars that produce significant numbers of LyC photons). For metallicities in the range  $0.002 \leq Z \leq 0.04$  (where  $Z = Z_{\odot} = 0.02$  is the solar metallicity) and for masses  $15 < m < 100$ , the fitted coefficients are  $B = 1.578$  and  $A(Z) = 0.0950 - 1.059Z$ . Thus, for  $Z = Z_{\odot} \approx 0.02$ , we have  $A = 0.0738$  and  $m_{\text{OB}} = 21.4 M_{\odot}$ , while for  $Z = 0.1Z_{\odot} = 0.002$  we have  $A = 0.0929$  and  $m_{\text{OB}} = 17 M_{\odot}$ . Inserting these values for  $Q(m)$  into equation (8), we integrate these LyC photon yields over the IMF, to derive the conversion coefficient,  $Q_{\text{LyC}}$ , from *total mass* in star formation to *total number* of LyC photons produced (in units of  $10^{63}$  photons per  $M_{\odot}$ ).

The integrals in eq. (8) can be done analytically as functions of the IMF parameters and metallicity. For a Salpeter IMF ( $\alpha = 2.35$ ,  $0.1 \leq m \leq 100$ ) we find:  $Q_{\text{LyC}} = 0.00236$  (for  $Z = Z_{\odot}$ ),  $Q_{\text{LyC}} = 0.00366$  (for  $Z = 0.2Z_{\odot}$ ), and  $Q_{\text{LyC}} = 0.00384$  (for  $Z = 0.1Z_{\odot}$ ). Adopting a typical (low- $Z$ ) value  $Q_{\text{LyC}} = 0.004$  ( $4 \times 10^{60}$  photons per  $M_{\odot}$ ), we can solve for the critical SFR for reionization, scaled to clumping factor  $C_H = 3$ , escape fraction  $f_{\text{esc}} = 0.2$ , and gas temperature  $T_4 = 1$ :

$$\dot{\rho}_{\text{crit}} = (0.018 M_{\odot} \text{ yr}^{-1} \text{ Mpc}^{-3}) \left[ \frac{(1+z)}{8} \right]^3 \left[ \frac{C_H/3}{f_{\text{esc}}/0.2} \right] \left[ \frac{0.004}{Q_{\text{LyC}}} \right] T_4^{-0.845}. \quad (9)$$

Our chosen value of  $C_H \approx 3$  is consistent with recent downward revisions (Pawlik et al. 2009) and with our numerical simulations discussed in Section 2.3. Escape fractions  $f_{\text{esc}} \approx 0.1 - 0.2$  have been inferred from observations at  $z \approx 3$  (Shapley et al. 2006; Nestor et al. 2011) and theoretical expectations (Fernandez & Shull 2011). Equation (9) agrees with prior estimates (Madau et al. 1999) when adjusted for our new scaling factors, in particular the ratio ( $C_H/f_{\text{esc}} = 15$ ). Their earlier paper assumed  $C_H = 30$ ,  $f_{\text{esc}} = 1$ ,  $\Omega_b h^2 = 0.020$ ,  $Q_{\text{LyC}} = 0.005$ , and  $z = 5$ . Our fiducial redshift has increased from  $z = 5$  to  $z = 7$ , appropriate for the new discoveries of high-redshift galaxy candidates for reionization. Expressed with the same coefficients in eq. (9), their coefficient would be nearly the same,  $0.020 M_{\odot} \text{ yr}^{-1} \text{ Mpc}^{-3}$  at  $z = 7$ . One of the improvements in our formulation is to better identify the dependences on the physical parameters ( $C_H$ ,  $f_{\text{esc}}$ ,  $T_e$ ) and the SFR-to-LyC conversion factor ( $Q_{\text{LyC}}$ ), which can change with different IMFs and atmospheres.

A related calculation is the production rate of ionizing (LyC) photons per unit volume, needed to balance hydrogen recombinations. With the same assumptions as above, this is

$$\left( \frac{dN_{\text{LyC}}}{dt} \right)_{\text{crit}} = n_e n_{\text{HII}} \alpha_H^{(B)} = (4.6 \times 10^{50} \text{ s}^{-1} \text{ Mpc}^{-3}) \left[ \frac{(1+z)}{8} \right]^3 T_4^{-0.845} \left( \frac{C_H}{3} \right). \quad (10)$$

For standard high-mass stars (O7 V, solar metallicity) each with LyC photon luminosity  $10^{49} \text{ s}^{-1}$ , this rate corresponds to an O-star space density  $n_O \approx 50 \text{ Mpc}^{-3}$  at  $z = 7$ . Schaerer

(2002, 2003) also computed models of Population III and low-metallicity stars based on non-LTE model atmospheres and new stellar evolution tracks and evolutionary synthesis models. The lifetime total number of LyC photons produced per star of mass  $m$  is  $Q(m) = \bar{Q}(H) \times t_*$ . For stars of mass parameter  $x = \log(m/M_\odot)$ , the number of ionizing photons,  $\bar{Q}$ , emitted per second per star, is given by:

$$\log_{10} [\bar{Q}_H/s^{-1}] = \begin{cases} 43.61 + 4.90x - 0.83x^2 & Z = 0, & 9 - 500M_\odot, \\ 39.29 + 8.55x & Z = 0, & 5 - 9M_\odot, \\ 27.80 + 30.68x - 14.80x^2 + 2.50x^3 & Z = 0.02Z_\odot, & 7 - 150M_\odot, \\ 27.89 + 27.75x - 11.87x^2 + 1.73x^3 & Z = Z_\odot, & 7 - 120M_\odot \end{cases} \quad (11)$$

and the star’s lifetime  $t_*$  is given by:

$$\log_{10} [t_*] = \begin{cases} 9.785 - 3.759x + 1.413x^2 - 0.186x^3 & Z = 0, \\ 9.59 - 2.79x + 0.63x^2 & Z = 0.02Z_\odot, \\ 9.986 - 3.497x + 0.894x^2 & Z = Z_\odot \end{cases} \quad (12)$$

Sample values of  $Q_{\text{LyC}}$  and  $\dot{\rho}_{\text{crit}}$  for different IMFs are shown in Table 1, for both model atmospheres. One can obtain different values of  $Q_{\text{LyC}}$  for power-law IMFs by varying their high-mass slope  $\beta$  and the minimum and maximum masses. Increases in  $Q_{\text{LyC}}$  translate into *decreases* in critical SFR. For example, at  $0.1 Z_\odot$ , if the minimum mass is raised to  $1 M_\odot$  with a Salpeter slope ( $\beta = 2.35$ ), the LyC production factor rises to  $Q_{\text{LyC}} = 0.0098$ , some 2.5 times higher than the equivalent model,  $Q_{\text{LyC}} = 0.00384$  for  $m_{\text{min}} = 0.1M_\odot$ . If the IMF is flatter,  $\beta = 2$  instead of 2.35, with minimum mass fixed at  $m_{\text{min}} = 0.1M_\odot$ ,  $Q_{\text{LyC}} = 0.0177$  (4.6 times higher). At the upper end of the IMF, if one increases  $m_{\text{max}}$  from 100 to 200  $M_\odot$ , keeping  $\beta = 2.35$  and  $m_{\text{min}} = 0.1$ , one finds  $Q_{\text{LyC}} = 0.0054$  (1.4 times higher). All of these variations can be explored with our reionization/SFR simulator, described in Section 3.3.

The critical SFR of  $0.018 M_\odot \text{ yr}^{-1} \text{ Mpc}^{-3}$  can be understood from simple arithmetic. Over the 386 Myr recombination time (eq. [6]) with  $C_H = 3$ ,  $f_{\text{esc}} = 0.2$ , and  $z = 7$ , approximately 20 million stars are formed per comoving  $\text{Mpc}^3$  in a Salpeter IMF ( $0.1 - 100 M_\odot$ ) with mean stellar mass  $0.352M_\odot$ . Of these stars, a small fraction,  $f_{\text{OB}} \approx 7 \times 10^{-4}$ , are massive OB stars ( $m > 20M_\odot$ ). At an average of  $2 \times 10^{63}$  LyC photons and escape fraction  $f_{\text{esc}} = 0.2$ , these  $\sim 14,000$  OB stars will produce a net (escaping)  $\sim 5 \times 10^{66}$  LyC photons over their lifetime. These photons are sufficient to ionize  $N_H = 5.6 \times 10^{66}$  hydrogen atoms  $\text{Mpc}^{-3}$ .



### 2.3. Clumping Factor from Cosmological Simulations

The simulations used in this study were performed with `Enzo`, an Eulerian adaptive mesh-refinement (AMR), hydrodynamical + N-body code (Bryan & Norman 1997; O’Shea et al. 2004, 2005). Smith et al. (2011) enhanced this code by adding new modules for star formation, primordial chemistry, and cooling rates consistent with ionizing radiation, metal transport, and feedback. The ionizing background is spatially constant and optically thin, but variable in redshift. At this stage, we have not implemented radiative transfer or spectral filtering by the IGM.

For the clumping factor calculation, we ran a simulation on a  $50h^{-1}$  Mpc static grid (“unigrid”) cube with  $1024^3$  cells, denoted as run 50\_1024\_2 in Table 1 of Smith et al. (2011). The radiative heating from the ionizing background plays an important role in determining the properties of the filamentary structure. As a filament is ionized and heated, its density drops and its temperature rises; both effects reduce the recombination rate. To study these effects, we ran four moderate-resolution ( $50h^{-1}$  Mpc unigrid cube with  $512^3$  cells) simulations with varying ionizing backgrounds, summarized in Table 2. After initial submission of this paper, we ran a  $1536^3$  simulation, to check convergence and assess the “cosmic variance” among eight sub-volumes of the  $1024^3$  and  $1536^3$  simulations. The standard UV background was taken from Haardt & Madau (2001), although we also explore new computations of high- $z$  SFRs by Trenti et al. (2010) and Haardt & Madau (2012). These four simulations were: (1) no photoionizing background; (2) UV background ramped up from  $z = 7$  to  $z = 6$  (run 50\_512\_2 from Smith et al. 2011); (3) UV background ramped up from  $z = 9$  to  $z = 8$ ; and (4) UV background ramped up from  $z = 9$  to  $z = 8$ , but twice as strong as in (3). Post-processing of the simulations was performed using the data analysis and visualization package, `yt`<sup>1</sup>, documented by Turk et al. (2011).

For regions of ionized hydrogen of density  $n_{\text{HII}}$ , we calculate the clumping factor,  $C_H$ . using two different methods. The first calculation, which has been used in some earlier studies, uses density weighting. In this “density field” (DF) method we define

$$C_{\text{DF}} = \frac{\langle n_{\text{HII}}^2 \rangle}{\langle n_{\text{HII}} \rangle^2}, \quad (13)$$

and average the density fields (quantities  $x_i$ , denoting either  $n_{\text{HII}}$  or  $n_{\text{HII}}^2$ ) where parameter averages are computed by summing over grid cells ( $j$ ), subject to various “cuts” on the IGM

---

<sup>1</sup><http://yt.enzotools.org/>

overdensity and gas temperature and weighted by factors,  $w_j$ ,

$$\langle x_i \rangle = \frac{\sum_j x_j w_j}{\sum_j w_j} . \quad (14)$$

In the second calculation, we compare the local recombination rate to the global average recombination rate, averaged over density and temperature in cells,

$$C_{\text{RR}} = \frac{\langle n_e n_{\text{HII}} \alpha_H^{(B)}(T) \rangle}{\langle n_e \rangle \langle n_{\text{HII}} \rangle \langle \alpha_H^{(B)}(T) \rangle} , \quad (15)$$

where again  $\langle x \rangle$  denotes a weighted average and  $\alpha_H^{(B)}(T)$  is the case-B radiative recombination rate coefficient for hydrogen, as tabulated by Osterbrock & Ferland (2006). We refer to this as the “recombination rate” (RR) method.

Because the purpose of the clumping factor is to correct for an enhanced recombination rate, we believe  $C_{\text{RR}}$  to be a more appropriate representation. The recombinations that are important to removing ionizing photons occur in the filamentary structure of the IGM, and the clumping factor should only be calculated in these structures. To assess the critical SFR necessary to maintain an ionized medium, we focus on grid cells that are significantly ionized. Because a negligible amount of recombination occurs in cells containing mostly neutral gas, these cells should not contribute to the clumping factor. If we do not exclude neutral gas, the clumping factor is extremely high ( $C_H \sim 100$ ) before the ionizing background is turned on. We find large density gradients between the neutral gas (uniformly distributed over the simulation) and the ionized gas. Because the clumping factor is a measure of the inhomogeneity of the medium, a large density gradient yields a large value of  $C_H$ . If low-density voids are included in the calculation, the larger density gradient leads to an overestimate of the clumping. By setting both upper and lower density thresholds, we can exclude collapsed halos and low-density voids from our calculations.

Previous studies (Miralda-Escudé 2000; Miralda-Escudé et al. 2003; Pawlik et al. 2009) addressed these issues by setting a density threshold that excludes collapsed halos, but they did not set a lower limit to exclude voids from their calculations. To explore these effects in a filamentary IGM, we make various cuts of our data in baryon overdensity ( $\Delta_b \equiv \rho_b / \bar{\rho}_b$ ) and in temperature, metallicity, and hydrogen ionization fraction ( $x \equiv n_{\text{HII}} / n_H$ ). In our standard formulation, we include only those cells that meet the following criteria:  $1 < \Delta_b < 100$ ,  $300 \text{ K} < T < 10^5 \text{ K}$ ,  $Z < 10^{-6} Z_\odot$ , and  $x > 0.05$ . We believe this “data cut” adequately represents unenriched IGM lying on an adiabat (see Figure 19 of Smith et al. 2011). We also explore the clumping factor with no lower density threshold (total range  $\Delta_b < 100$ ). Our results, presented in Section 3.1, show a small increase in  $C_H(z)$  from the wider range

in densities by including low-density cells with  $\Delta_b < 1$ . However, these low-density voids do not contribute substantially to the recombination rate.

In summary, our prescriptions for calculating the clumping factor yield a more physical representation of the enhanced recombination rate that is an important component to many reionization models. By not assuming a fully ionized medium and by specifically following  $n_{\text{HII}}$ , we are able to exclude denser neutral gas that does not contribute appreciably to the recombination rate. We make simple assumptions on the reionization process and reionization history (Section 3.2), turning on the ionizing radiation field at redshifts  $z = 7$  or  $z = 9$  and following the thermal history arising from photoelectric heating, radiative cooling, and pressure smoothing (Pawlik et al. 2009). The metal-line and molecular cooling, metal transport, and feedback included in our simulations also allow us to accurately represent the thermodynamics of the gas, which has been shown to have a significant effect on the evolution of the clumping factor. Future models will include discrete sources and radiative transfer, accounting for temperature increases arising from photo-heating with spectral hardening (Abel & Haehnelt 1999). Because our current simulations employ a spatially constant ionizing radiation field, we anticipate carrying out these more realistic situations.

### 3. RESULTS FROM SIMULATIONS

#### 3.1. Computing the Clumping Factor

Early studies of IGM clumping adopted high values,  $C_H > 40$  at  $z < 5$  (Gnedin & Ostriker 1997). As discussed earlier, we believe these values are too high for the ionized IGM filaments, which have expanded as a result of the heat deposited by LyC photons. The differences between observations and inferred critical SFR densities can largely be attributed to this high clumping factor (Sawicki & Thompson 2006; Bouwens et al. 2007). More recent studies have trended towards less clumping. Raičević & Theuns (2011) argue that using a global clumping factor overestimates the recombination rate, and that local values should be used instead. In this study, we calculate the clumping factor for a series of high-resolution cosmological simulations for ionized hydrogen and helium that explore how the photoheating of an ionizing background affects the IGM thermodynamics (density and temperature). We impose criteria in overdensity, temperature, metallicity, and ionization fraction to constrain our calculations to IGM filaments where recombinations and ionization fronts are most important. The clumping in simulation 50\_1024\_7 is calculated as a function of redshift from  $z = 15$  to  $z = 0$  for both  $C_{\text{DF}}$  and  $C_{\text{RR}}$ , weighted by overdensity and by volume. Note that the unigrid simulations automatically yield volume weighting, when averaged over cells. For the remainder of our simulations, we find a power-law overdensity distribution, with an

average form  $f(\Delta_b) = 10^6 \Delta_b^{-1.5}$ . Weighting these cells by overdensity gives undue emphasis on small numbers of high-density cells. This method is also biased, since it does not calculate the clumping factor where most of the recombinations are occurring.

Figure 1 compares the DF and RR methods and shows the difference between the different weights used in our calculations. In both methods, weighting by overdensity results in higher clumping factors. The recombination-rate method (eq. [15]) results in a lower clumping factor because it accounts for both density and temperature effects from the ionizing background on the clumping averages. Photoelectric heating during photoionization causes the filaments to expand, lowering the density. The increased electron temperature also reduces the radiative recombination rate coefficient. The DF method (eq. [13]) includes no dependence on the recombination rate coefficient, and therefore only counts the effect of photoheating on the filament density. See Section 3.2 for further discussion.

In our current simulations, we turn on a spatially constant UV background at  $z = 7$  or  $z = 9$ . The effects of different “density cuts” in the summation over cells (see Section 2.3) are shown in Figure 2. We find little difference at  $z > 9$  (turn-on of ionizing radiation), and see a small increase in  $C_H$  at  $z < 9$  when we include the lower density cells with  $\Delta_b < 1$ . In future, more refined simulations with radiative transfer, we expect photoionization to be initiated in high-density regions, where the stars are located. Once the UV background is turned on, lower-density regions are easily photoionized. The photoelectric heating of the UV background causes the filaments to expand and become diffuse, resulting in a lower clumping factor. The elevated temperature also reduces the recombination rate coefficient, which in turn lowers  $C_H$  when calculated by the RR method. When calculating a mean recombination rate, only the recombining ionized gas is relevant. By  $z \sim 6$ , the IGM is nearly completely ionized and only small regions of H I remain. As noted earlier, in more refined simulations, the remaining H I would be largely self-shielded from the UV background and likely to reside in clumps of high density yet unreached by ionization fronts.

Figure 3 explores the convergence and cosmic variance among different simulations. In two panels, we compare results from our  $512^3$  simulations with larger simulations with  $1024^3$  and  $1536^3$  cells. In each panel, we show the average clumping factors, together with those in eight sub-volumes. The average values of  $C_H$  agree in the  $1024^3$  and  $1536^3$  simulations, and the small ( $\pm 10\%$ ) variance among these sub-volumes suggests that the  $1024^3$  and  $1536^3$  simulations are converged. Over the redshift range  $5 < z < 9$  in the  $1536^3$  simulation, the clumping factor is well fitted by a power-law,

$$C_H(z) = (2.9) \left[ \frac{(1+z)}{6} \right]^{-1.1}, \quad (16)$$

representing a slow rise in clumping to lower redshift, after the turn-on of ionizing radiation.

### 3.2. Ionizing Background Study

To study the effect of radiative heating from the ionizing background on filamentary structure, we ran a suite of moderate-resolution simulations with different ionizing backgrounds (see Table 2 for details). The redshift at which the UV background is turned on affects the clumping factor, causing it to drop and then recover at lower redshift. Pawlik et al. (2009) attribute this effect to *Jeans filtering*, where the photo-heating raises the cosmological Jeans mass, preventing further accretion onto low-mass halos and smoothing out small-scale density fluctuations. The photoheating also heats the filaments we are focusing on, which lowers the hydrogen recombination rate coefficient,  $\alpha_H^{(B)} \propto T^{-0.845}$ , and causes the filaments to expand; both of these effects reduce the clumping factor. Without a UV background, the clumping continues to rise as the filaments gravitationally collapse. Pawlik et al. (2009) also claim that the clumping factor at  $z = 6$  is insensitive to when the background is turned on, as long as it is turned on at  $z > 9$ . When an ionizing background is introduced, photoheating acts as a positive feedback to reionization by lowering the clumping factor and making it easier to stay ionized. This same photoheating mechanism also suppresses star formation in low-mass halos, which in turn lowers the ionizing photon production rate by star-forming galaxies and acts as a negative feedback to reionization (Pawlik et al. 2009). These thermodynamic processes affect clumping and structure and emphasize the importance of carefully modeling the strength of feedback processes and their effects on Jeans mass.

We have explored what happens when the ionizing radiation turned on earlier, especially during the interval  $z = 6 - 8$  marking the transition from a neutral to fully ionized IGM. In a series of 512<sup>3</sup> simulations, we explore the influence of turn-on of photoionizing radiation between redshifts  $z = 7$  and  $z = 9$ . Figure 4 shows  $C_H$ , computed for the moderate-resolution simulations via the density-field method and weighted by volume. We do not plot simulation 50\_512\_9\_2, since it is identical to simulation 50\_512\_9. As in the results of Pawlik et al. (2009), we find that photoheating from the ionizing background results in a decrease in the clumping factor. The clumping factors fall along two tracks: a higher track at redshifts above the turn-on of the UV background, and a lower one after turn-on. By  $z = 5$ , we find nearly identical clumping factors for both backgrounds. After a substantial recovery time, the redshift when the background is turned on is not important. Before this recovery, the clumping factor of the earlier background is lower by a factor of  $\sim 2$ , resulting in earlier reionization.

One can compare the strengths of feedback to reionization, where “positive feedback” lowers the clumping factor and “negative feedback” suppresses star formation. At  $z = 5$  the total stellar mass (SFR density) of simulation 50\_512\_7 is 1.19 (1.13) times lower than that of simulation 50\_512\_0, while the clumping factor is 1.64 times lower. For simulation

50\_512\_9, the total stellar mass (SFR density) and clumping factor are 1.52 (1.49) and 1.66, respectively, times lower than those of simulation 50\_512\_0. This suggests that the positive feedback introduced by the background is greater than the negative feedback. However, the stellar mass (SFR density) does not recover in the same manner as the clumping factor. Once photoheating suppresses the formation of small-mass halos, the Hubble flow takes over and prevents them from collapsing and forming stars. Therefore, the redshift at which the background is turned on determines whether the positive or negative feedback dominates and whether the ionizing background will cause reionization to be accelerated or delayed.

### 3.3. Reionization SFR Simulator

In connection with this project, we have developed a user interface for calculating the critical SFR density ( $\dot{\rho}_{\text{crit}}$ ) needed to maintain the IGM ionization at a given redshift. The software computes the effects of variations in the stellar IMF (slope, mass-range) and model atmospheres, and the redshift evolution of metallicity and gas thermodynamics (density, temperature, coupling to the CMB). The clumping factor and LyC escape fraction are free parameters in the calculator. Our simulations find ranges of  $C_H \approx 1 - 10$  depending on redshift, overdensity, and thermal phase of the (photoionized or shock-heated) IGM. For the new 1536<sup>3</sup> simulation, the global mean clumping factor is  $\langle C_H \rangle \approx 3$ , with a power-law fit  $C_H(z) = (2.9)[(1+z)/6]^{-1.1}$  for redshifts between  $5 < z < 9$ .

This calculator is a useful tool for determining the population of galaxies responsible for reionization. The critical SFR per co-moving volume (Eq. [9]) is obtained by balancing the production rate of LyC photons with the number of hydrogen recombinations. Here,  $C_H$  is the clumping factor of ionized hydrogen,  $f_{\text{esc}}$  is the escape fraction of LyC photons from their host galaxies, and  $T_4$  is the temperature scaled to  $10^4$  K. The conversion factor,  $Q_{\text{LyC}}$ , from stellar mass to total number of LyC photons produced, is regulated by the IMF and model atmospheres. The user has the option of controlling these parameters to determine the resulting critical SFR density, subject to several observational constraints. This simulator can be accessed at <http://casa.colorado.edu/~harnessa/SFRcalculator> with an html interface for easy use.

Two standard tests of the SFR use the simulator to calculate the ionization histories of H II and He III and compare them to the ionized volume filling factor,  $Q_{\text{HII}}(z)$ , and the CMB optical depth,  $\tau_e(z)$ . The calculator derives  $\tau_e(z)$  by integrating the differential form of Eq. (3) for various SFR histories and parameters. The average evolution of  $Q_{\text{HII}}$  is found by numerical integration of the rate equation (Madau, Haardt, & Rees 1999) expressing the



sources and sinks of ionized zones,

$$\frac{dQ_{\text{HII}}}{dt} = \frac{\dot{n}_{\text{LyC}}}{\langle n_H \rangle} - \frac{Q_{\text{HII}}}{\langle t_{\text{rec}}(C_H) \rangle}. \quad (17)$$

The source term,  $\dot{n}_{\text{LyC}} = \dot{\rho}_{\text{SFR}} f_{\text{esc}} Q_{\text{LyC}}$ , represents the net ionizing photon production rate, computed from selected models of the SFR density,  $\dot{\rho}_{\text{SFR}}$ . Here,  $\langle n_H \rangle$  is the mean hydrogen number density, and  $\langle t_{\text{rec}} \rangle$  is the hydrogen recombination timescale, which depends on  $C_H$  as shown in Eq. (6). The IGM is assumed to be fully ionized when  $Q_{\text{HII}} = 1$ . We integrate a similar equation for  $Q_{\text{HeIII}}$  to follow He II photoionization in the QSO 4-ryd continuum. We use the QSO emissivities at 1 ryd (Haardt & Madau 2012), extrapolated to 4 ryd assuming a spectrum with specific flux  $F_\nu \propto \nu^{-1.8}$ .

Figure 5 shows ionization histories, quantified by  $Q_{\text{HII}}(z)$  and  $\tau_e(z)$ , for various values of clumping factor, escape fraction, IGM temperature, and LyC-production efficiencies ( $Q_{\text{LyC}}$ ). We adopt the SFR history from Trenti et al. (2010) with an evolving luminosity function. Our standard model adopts  $C_H = 3$ ,  $f_{\text{esc}} = 0.2$ ,  $T_4 = 2$ , and  $Q_{\text{LyC}} = 0.004$  ( $4 \times 10^{60}$  photons/ $M_\odot$ ). Different curves show the effects of changing  $C_H$  and  $f_{\text{esc}}$ , including two models in which these parameters evolve with redshift. With these parameters, we are typically able to complete reionization by  $z \approx 7$ , consistent with observations of Gunn-Peterson troughs, redshift evolution in Ly $\alpha$  emitters, and IGM neutral fraction. The model with a constant  $f_{\text{esc}} = 0.05$  does not complete the ionization until  $z \approx 4$ , which is far too late. Thus, we believe that LyC escape fractions must be considerably larger ( $\geq 20\%$ ) perhaps evolving to higher values at  $z > 6$  shown by green and magenta curves.

Figure 6 compares the dependence of  $Q_{\text{HII}}(z)$  and  $\tau_e(z)$  on SFR histories, computed with an evolving luminosity function (Trenti et al. 2010) and new calculations (Haardt & Madau 2012) of the star formation rate density,  $\dot{\rho}_{\text{SFR}}(z)$ . Figure 7 compares the effects of two choices of model atmospheres, with a fixed SFR history from Trenti et al. (2010). The on-line calculator provides ionization fractions,  $Q_{\text{HII}}(z)$  and  $Q_{\text{HeIII}}(z)$ , together with CMB optical depth,  $\tau_e(z)$ . In the simulator, users can select other IGM parameters and SFR histories. The main difference between the two SFR models lies in the assumptions at  $z > 8$ . Haardt & Madau (2012) rely on an empirical extrapolation of the star formation rate as a function of redshift, while Trenti et al. (2010) adopt a physically motivated model based on the evolution of the dark-matter halo mass function. The two approaches are similar at  $z \lesssim 8$ , but differ significantly at higher redshift, where an empirical extrapolation does not capture the sharp drop in the number density of galaxies observed at  $z \sim 10$  (see Figure 8 in Oesch et al. 2011). As a consequence, the reionization history from the Haardt & Madau (2012) model is more extended at high  $z$ , especially when the efficiency of reionization is increased because of evolving clumping factor and escape fraction (our preferred models, green and magenta curves in Fig. 5). The two models yield quite different predictions for the duration

of reionization, defined as the redshift interval,  $\Delta z$ , over which  $Q_{\text{HII}}$  evolves from 20% to 80% ionized. Our preferred SFR models (green and magenta lines in Fig. 5) have  $\Delta z \approx 3$  (from  $z \approx 10.5$  to  $z \approx 7.5$ ), whereas the Haardt-Madau SFR histories exhibit a more extended interval,  $\Delta z \approx 6$  (from  $z \approx 13$  to  $z \approx 7$ ). This difference in  $\Delta z$  could be tested by upcoming 21-cm experiments; see Bowman & Rodgers (2010) for an initial constraint,  $\Delta z > 0.06$ .

Figure 8 illustrates a third constraint on the reionization epoch (Pritchard et al. 2010; Lidz et al. 2011) comparing SFR histories with estimates of the ionizing background at  $z = 5.5 \pm 0.5$  (Fan et al. 2006; Bolton & Haehnelt 2007; Haardt & Madau 2012). The LyC co-moving emissivity (in photons  $\text{s}^{-1} \text{Mpc}^{-3}$ ), defined as  $\dot{n}_{\text{LyC}} = \dot{\rho}_{\text{SFR}} f_{\text{esc}} Q_{\text{LyC}}$ , can be related to the ionizing background at  $z = 5 - 6$ , using recent estimates of the hydrogen photoionization rate,  $\Gamma_{\text{HI}}(z)$ , from Haardt & Madau (2012) and the LyC mean free path,  $\lambda_{\text{HI}}$ , from Songaila & Cowie (2010). The LyC emissivity is proportional to the star formation rate density, computed from our halo mass function model (Trenti et al. 2010), integrated down to absolute magnitudes  $M_{\text{AB}} = -18$  (Bouwens et al. 2011a) or to  $M_{\text{AB}} = -10$ , the faint limit suggested by Trenti et al. (2010). We adopt a fiducial LyC production parameter  $Q_{\text{LyC}} = 0.004$ , corresponding to  $4 \times 10^{60}$  LyC photons produced per  $M_{\odot}$  of star formation, and we use two different models for LyC escape fraction,  $f_{\text{esc}}$  (constant at 20% and varying with redshift). For quantitative values, we assume an ionizing background with specific intensity,  $J_{\nu} = J_0(\nu/\nu_0)^{-\alpha}$  (in units  $\text{erg cm}^{-2} \text{s}^{-1} \text{sr}^{-1} \text{Hz}^{-1}$ ) with power-law index  $\alpha \approx 2$  at energies above  $h\nu_0 = 1$  ryd. The hydrogen photoionization rate is  $\Gamma_{\text{HI}} = [4\pi J_0 \sigma_0 / h(\alpha + 3)]$  for a hydrogen photoionization cross section  $\sigma_{\nu} \approx \sigma_0(\nu/\nu_0)^{-3}$  with  $\sigma_0 = 6.3 \times 10^{-18} \text{cm}^2$ . For this spectrum, the frequency-integrated ionizing intensity is  $J_{\text{tot}} = J_0 \nu_0 / (\alpha - 1)$ , and the LyC photon flux (photons  $\text{cm}^{-2} \text{s}^{-1}$ ) integrated over all solid angles is  $\Phi_{\text{LyC}} = (4\pi J_0 / h\alpha)$ . Because we analyze the *photon* mean-free path, we normalize  $J_0$  to  $\Phi_{\text{LyC}}$  and  $\Gamma_{\text{HI}}$ ,

$$J_0 = \frac{h\alpha\Phi_{\text{LyC}}}{4\pi} = \frac{h(\alpha + 3)}{4\pi\sigma_0} \Gamma_{\text{HI}}. \quad (18)$$

By approximating  $\Phi_{\text{LyC}}$  as the product of the LyC emissivity and mean-free path, we arrive at the calibrations:

$$J_{\text{tot}} = \frac{h\nu_0}{4\pi\sigma_0} \frac{(\alpha + 3)}{(\alpha - 1)} \Gamma_{\text{HI}} = (6.88 \times 10^{-7} \text{ erg cm}^{-2} \text{ s}^{-1} \text{ sr}^{-1}) \left[ \frac{\Gamma_{\text{HI}}}{5 \times 10^{-13} \text{ s}^{-1}} \right] \quad (19)$$

$$\Phi_{\text{LyC}} = \frac{(\alpha + 3)}{\alpha} \frac{\Gamma_{\text{HI}}}{\sigma_0} = (1.98 \times 10^5 \text{ photons cm}^{-2} \text{ s}^{-1}) \left[ \frac{\Gamma_{\text{HI}}}{5 \times 10^{-13} \text{ s}^{-1}} \right]. \quad (20)$$

Finally, we relate  $\Phi_{\text{LyC}}$  to the star-formation rate  $\dot{\rho}_{\text{SFR}}$  and ionization rate  $\Gamma_{\text{HI}}$ ,

$$\dot{\rho}_{\text{SFR}} = (0.056 M_{\odot} \text{ yr}^{-1} \text{ Mpc}^{-3}) \left[ \frac{\Gamma_{\text{HI}}}{5 \times 10^{-13} \text{ s}^{-1}} \right] \left[ \frac{0.1}{f_{\text{esc}}} \right] \left[ \frac{0.004}{Q_{\text{LyC}}} \right] \left[ \frac{9.8 \text{ pMpc}}{\lambda_{\text{HI}}} \right] \left[ \frac{6.5}{1+z} \right]^3. \quad (21)$$

Here, we have scaled the parameters to the same values assumed by Lidz et al. (2011), namely  $\Gamma_{\text{HI}} = 5 \times 10^{-13} \text{ s}^{-1}$ ,  $f_{\text{esc}} = 0.1$ , an ionizing spectral index  $\alpha = 2$ , and redshift  $z = 5.5$ , at which Songaila & Cowie (2010) fit  $\lambda_{\text{HI}} \approx 9.8$  proper Mpc. Our parameter  $Q_{\text{LyC}} = 0.004$  corresponds to the Lidz et al. (2011) LyC photon production calibration,  $10^{53.1} \text{ s}^{-1}$  per  $M_{\odot} \text{ yr}^{-1}$  of star formation. However, our coefficient,  $0.056 M_{\odot} \text{ yr}^{-1} \text{ Mpc}^{-3}$ , is slightly larger than their value,  $0.039 M_{\odot} \text{ yr}^{-1} \text{ Mpc}^{-3}$ , an effect that may arise from our different method of relating  $\Gamma_{\text{HI}}$  to the ionizing radiation field and SFR.

More careful examination of these parameters suggests that, at  $z \approx 5.5$ , the hydrogen ionization rate  $\Gamma_{\text{HI}} \approx 3.6 \times 10^{-13} \text{ s}^{-1}$ , given in Table 3 of Haardt & Madau (2012), and the observed mean free path,  $\lambda_{\text{HI}}$ , at  $z = 5.5$  may be closer to 6 proper Mpc (see Figure 10 of Songaila & Cowie 2010). Rescaling to those two parameters, we find a similar coefficient of  $0.066 M_{\odot} \text{ yr}^{-1} \text{ Mpc}^{-3}$ . This SFR density at  $z = 5.5 \pm 0.5$  (see also Figure 8) is comparable to the critical value needed to maintain reionization at  $z = 7$ , but the observed rates and mean free paths are declining rapidly with redshift. All three constraints on SFR suggest that full reionization is more likely to occur at redshift  $z_{\text{rei}} \approx 7$  than at  $z_{\text{rei}} = 10$ .

#### 4. DISCUSSION AND IMPLICATIONS

The major results of our study can be summarized with the following points:

1. We calculated the critical star formation rate required to maintain a photoionized IGM, incorporating four free parameters ( $C_H$ ,  $f_{\text{esc}}$ ,  $T_e$ ,  $Q_{\text{LyC}}$ ) that control the rates of LyC photon production and radiative recombination. Our best estimate at  $z = 7$  is  $\dot{\rho}_{\text{crit}} \approx (0.018 M_{\odot} \text{ yr}^{-1} \text{ Mpc}^{-3})[(1+z)/8]^3 (C_H/3)(0.2/f_{\text{esc}})T_4^{-0.845}$  for fiducial values of IGM clumping factor  $C_H = 3$ , LyC escape fraction  $f_{\text{esc}} = 0.2$ , temperature  $T_e = 10^4 \text{ K}$ , and standard IMFs and low-metallicity stellar atmosphere ( $Q_{\text{LyC}} = 0.004$ ).
2. An epoch of full reionization at  $z_{\text{rei}} \approx 7$  is consistent with recent optical/IR measurements of SFR history and a rising IGM neutral fraction at  $z = 6 - 8$ , marking the tail end of reionization. These observations include the decrease in numbers of high- $z$  galaxies and Ly $\alpha$  emitters and IGM damping-wing intrusion into the Ly $\alpha$  transmission profiles in high- $z$  QSOs.
3. Our newly developed SFR and reionization calculator, now available on-line at <http://casa.colorado.edu/~harnessa/SFRcalculator>, allows users to calculate the ionization history, critical SFR, and CMB optical depth, and to assess whether observed SFRs, IMFs, and other parameters are consistent with IGM reionization.

4. Reconciling late reionization at  $z_{\text{rei}} \approx 7$  with  $\tau_e = 0.088 \pm 0.015$  of the CMB likely requires an epoch of partial ionization. A fully ionized IGM back to  $z_{\text{rei}} = 7$  produces  $\tau_e \approx 0.050$ , and an additional optical depth,  $\Delta\tau_e \approx 0.01 - 0.04$ , may arise from early sources of UV/X-ray photons at  $z > 7$ . Alternatively, one can appeal to the likelihood contours from WMAP, which allow optical depths as low as 0.06 (95% C.L.) The *Planck* experiment may clarify the situation in several years.
5. If the EoR is more complex, as we suggest, then redshifted 21-cm experiments should focus on the interval  $7.5 < z < 10.5$ , corresponding to frequencies 124–167 MHz, for the maximum signal of IGM heating ( $T_b \approx 27$  mK) produced when the hydrogen neutral fraction  $x_{\text{HI}} \approx 0.5$  (Pritchard et al. 2010).

We conclude by speculating about which future observations can best constrain the EoR. Additional data from the *Planck* mission<sup>2</sup> should provide confirmation of the CMB optical depth with smaller error bars. This information will constrain the additional amount of ionization at  $z > 7$  and narrow the range  $\Delta\tau_e = 0.01 - 0.04$  produced by high-redshift sources in the partially ionized IGM. Ongoing surveys for high- $z$  galaxies, Ly $\alpha$  emitters, and QSO near-zone sizes will better quantify the rise of neutral fraction,  $x_{\text{HI}}$  at  $z > 6.5$ . On the theoretical front, we are running larger IGM simulations on  $1536^3$  and  $2048^3$  unigrids and will add discrete sources of ionizing radiation and radiative transfer in order to capture the heating and clumping more accurately. We will also include source turn-on at  $z > 9$  to test the decrease and recovery of  $C_H$ , as seen in Figures 3 and 4. Finally, we plan to carry out more detailed modeling of the H I (21-cm) signal, coupled to the kinetic and spin temperatures driven by heating at  $z > 7$ . As described earlier, the duration of the reionization transition and the 21-cm emission during the heating phase could provide discriminants of various SFR histories at  $z > 6$ .

This work was supported by grants to the Astrophysical Theory Program (NNX07-AG77G from NASA and AST07-07474 from NSF) at the University of Colorado Boulder. We thank Joanna Dunkley, Chris Carilli, Richard Ellis, and Piero Madau for useful discussions on reionization and CMB optical depth statistics. We are grateful to the referee for suggesting additional model comparisons with the ionizing background at  $z = 5 - 6$ .

---

<sup>2</sup>See mission website <http://www.rssd.esa.int/Planck>

## REFERENCES

- Abel, T., & Haehnelt, M. G. 1999, *ApJ*, 520, L13
- Abel, T., Bryan, G., & Norman, M. L. 2002, *Science*, 295, 93
- Becker, G. D., Rauch, M., & Sargent, W. L. W. 2007, *ApJ*, 662, 72
- Becker, G. D., Bolton, J. S., Haehnelt, M. G., & Sargent, W. L. W. 2011, *MNRAS*, 410, 1096
- Benson, A. J., Sugiyama, N., Nusser, A., & Lacey, C. G. 2006, *MNRAS*, 369, 1055
- Bolton, J., & Haehnelt, M. 2007, *MNRAS*, 382, 325
- Bouwens, R. J., Illingworth, G. D., Franx, M., & Ford, H. 2007, *ApJ*, 670, 928
- Bouwens, R. J., Illingworth, G. D., Oesch, P., et al. 2009, *ApJ*, 705, 936
- Bouwens, R. J., Illingworth, G. D., Oesch, P., et al. 2010a, *ApJ*, 708, L69
- Bouwens, R. J., Illingworth, G. D., Oesch, P., et al. 2010b, *ApJ*, 709, L133
- Bouwens, R. J., Illingworth, G. D., Labbé, I., et al. 2011a, *Nature*, 469, 504
- Bouwens, R. J., Illingworth, G. D., Oesch, P., et al. 2011b, *ApJ*, submitted (arXiv:1105:2038)
- Bouwens, R. J., Illingworth, G. D., Oesch, P., et al. 2011c, *ApJ*, 737, 90
- Bowman, J. D., & Rogers, A. E. E. 2010, *Nature*, 468, 796
- Bromm, V., & Loeb, A. 2003, *Nature*, 425, 812
- Bryan, G. L., & Norman, M. L. 1997, in *Workshop on AMR Methods*, astro-ph/9710187
- Carilli, C. L., Wang, R., Fan, X., et al. 2010, *ApJ*, 714, 834
- Cen, R. 2003, *ApJ*, 591, 12
- Choudhury, T. R., & Ferrara, A. 2005, *MNRAS*, 361, 577
- Davé, R., Cen, R., Ostriker, J. P., et al. 2001, *ApJ*, 552, 473
- Dove, J. B., & Shull, J. M. 1994, *ApJ*, 430, 222
- Fan, X., Narayanan, V. K., Lupton, R. H., et al. 2001, *AJ*, 122, 2833
- Fan, X., Carilli, C. L., & Keating, B. 2006, *ARA&A*, 44, 415
- Fernandez, E. R., & Shull, J. M., 2011, *ApJ*, 731:20
- Gnedin, N. Y., & Ostriker, J. P. 1997, *ApJ*, 486, 581
- Gnedin, N. Y., & Fan, X., 2006, *ApJ*, 648, 1
- González, V., Labbé, I., Bouwens, R. J., et al. 2010, *ApJ*, 713, 115

- Gunn, J. E., & Peterson, B. A., 1965, *ApJ*, 142, 1633
- Haardt, F., & Madau, P. 2001, in *Clusters of Galaxies and the High Redshift Universe Observed in X-rays*, ed. D. M. Neumann & J. T. V. Tran (Saclay: CEA)
- Haardt, F., & Madau, P. 2012, *ApJ*, in press (arXiv:1105.2039)
- Hopkins, A. M., & Beacom, J. F. 2006, *ApJ*, 651, 142
- Hu, E. M., & Cowie, L. L. 2006, *Nature*, 440, 1145
- Kashikawa, N., Shimasaku, K., Matsuda, Y., et al. 2011, *ApJ*, 734, 119
- Kohler, K., Gnedin, N. Y., & Hamilton, A. J. S. 2007, *ApJ*, 657, 15
- Komatsu, E., Smith, K. M., Dunkley, J., et al. 2011, *ApJS*, 192:18
- Larson, D., Hinshaw, G., Komatsu, E., et al. 2011, *ApJS*, 192:16
- Lidz, A., Furlanetto, S., Oh, S. P., Aguirre, J., Chang, T.-C., Doré, O., & Pritchard, J. R. 2011, *ApJ*, 741:70
- Lidz, A., Zahn, O., McQuinn, M., Zaldarriaga, M., & Hernquist, L. 2008, *ApJ*, 680, 962
- Madau, P., Haardt, F., & Rees, M. J. 1999, *ApJ*, 514, 648
- Miralda-Escudé, J. 2003, *ApJ*, 597, 66
- Miralda-Escudé, J., Haehnelt, M., & Rees, M. J. 2000, *ApJ*, 530, 1
- Mortlock, D. J., Warren, S. J., Venemans, B. P., et al. 2011, *Nature*, 474, 616
- Nestor, D., Shapley, A. E., Steidel, C. C., & Siana, B. 2011, *ApJ*, 736:18
- Oesch, P., Bouwens, R., Illingworth, G., et al. 2011, *ApJ*, submitted (arXiv:1105.2297)
- Ono, Y., Ouchi, M., Mobasher, B., et al. 2012, *ApJ*, in press (arXiv:1107.3159)
- O’Shea, B., Bryan, G., Bordner, J., et al. 2004, in *Adaptive Mesh Refinement*, Springer, astro-ph/0403044, *Introducing Enzo, an AMR Cosmology Application*
- O’Shea, B. W., Nagamine, K., Springel, V., Hernquist, L., & Norman, M. L. 2005, *ApJS*, 160, 1
- Osterbrock, D. E., & Ferland, G. J. 2006, *Astrophysics of Gaseous Nebulae and Active Galactic Nuclei*, (Sausalito, CA: Univ. Science Books).
- Ouchi, M., Shimasaku, K., Furusawa, H., et al. 2010, *ApJ*, 723, 869
- Pawlik, A. H., Schaye, J., & van Scherpenzeel, E. 2009, *MNRAS*, 394, 1812
- Peimbert, M., Luridiana, V., & Peimbert, A. 2007, *ApJ*, 666, 636
- Pritchard, J. R., Loeb, A., & Wyithe, J. S. B. 2010, *MNRAS*, 408, 57



- Raičević, M., & Theuns, T. 2011, MNRAS, 412, L16
- Ricotti, M., & Ostriker, J. P. 2004, MNRAS, 352, 547
- Robertson, B. E., Ellis, R. S., Dunlop, J. S., McLure, R. J., & Stark, D. P. 2010, Nature, 468, 49
- Sawicki, M., & Thompson, D. 2006, ApJ, 648, 299
- Schaerer, D. 2002, A&A, 382, 28
- Schaerer, D. 2003, A&A, 397, 527
- Schenker, M. A., Stark, D. P., Ellis, R. S., et al. 2012, ApJ, in press (arXiv:1107.1261)
- Shapley, A. E., Steidel, C. C., Pettini, M., Adelberger, K. L., & Erb, D. K. 2006, ApJ, 651, 688
- Shull, J. M., & Venkatesan, A. 2008, ApJ, 685, 1
- Shull, J. M., France, K., Danforth, C. W., Smith, B. D., & Tumlinson, J. 2010, ApJ, 722, 1312
- Smith, B. D., Turk, M., Sigurdsson, S., O’Shea, B., & Norman, M. L. 2009, ApJ, 691, 441
- Smith, B. D., Hallman, E., Shull, J. M., & O’Shea, B. 2011, ApJ, 731:6
- Songaila, A. 2004, AJ, 127, 2598
- Sunyaev, R. 1977, Akademia Nauk USSR, Astr. J. Letters, 3, 491
- Trac, H., & Cen, R. 2007, ApJ, 671, 1
- Trenti, M., & Shull, J. M. 2010, ApJ, 712, 435
- Trenti, M., Stiavelli, M., Bouwens, R. J., et al. 2010, ApJ, 714, L202
- Tumlinson, J. 2007, ApJ, 664, L63
- Turk, M. J., Smith, B. D., Oishi, J. S., et al. 2011, ApJS, 192:9
- Venkatesan, A., Tumlinson, J., & Shull, J. M. 2003, ApJ, 584, 621

Table 1. Sample values of  $Q_{\text{LyC}}$  and  $\dot{\rho}_{\text{crit}}$  for different IMFs

$M_{\text{min}} (M_{\odot})$	$M_{\text{max}} (M_{\odot})$	$\alpha$	$Z$	$Q_{\text{LyC}}^{\text{a}}$	$Q_{\text{LyC}}^{\text{b}}$	$\dot{\rho}_{\text{crit}}^{\text{a}}$	$\dot{\rho}_{\text{crit}}^{\text{b}}$
0.1	100	2.35	$Z_{\odot}$	0.00236	0.00286	0.0306	0.0253
0.1	100	2.35	$0.02Z_{\odot}$	0.00397	0.00558	0.0181	0.0129
0.1	100	2.35	0	0.00401	0.00752	0.0180	0.0096
0.1	100	2.35	$0.2Z_{\odot}$	0.00365	...	0.0197	...
0.1	100	2.35	$0.1Z_{\odot}$	0.00383	...	0.0188	...
1.0	100	2.35	$0.1Z_{\odot}$	0.00976	...	0.0074	...
0.1	100	2.00	$0.1Z_{\odot}$	0.01267	...	0.0057	...
0.1	200	2.35	$0.1Z_{\odot}$	0.00543	...	0.0133	...

<sup>a</sup>Sutherland & Shull unpublished model atmospheres

<sup>b</sup>Schaerer model atmospheres

Note. — Production efficiency of ionizing (LyC) radiation,  $Q_{\text{LyC}}$ , in units of  $10^{63}$  photons/ $M_{\odot}$ . Critical SFR,  $\dot{\rho}_{\text{crit}}$ , is given in units of  $M_{\odot} \text{ yr}^{-1} \text{ Mpc}^{-3}$  (comoving) assuming  $C_H = 3$ ,  $f_{\text{esc}} = 0.2$ , and  $T_4 = 1$ .

Table 2. Parameters of Simulations

Run	$l$ ( $h^{-1} \text{ Mpc}$ )	$N_{\text{cells}}^{1/3}$	$z_{\text{UV}}$	Relative Strength of Background
50_1024_7 <sup>a</sup>	50	1024	7	1
50_512_7 <sup>b</sup>	50	512	7	1
50_512_9	50	512	9	1
50_512_9_2	50	512	9	2
50_512_0	50	512	N/A	0
50_1536_9	50	1536	9	1

<sup>a,b</sup>Simulations 50\_1024\_2, 50\_512\_2 from Smith et al. (2011).

Note. —  $z_{\text{UV}}$  is the redshift at which the ionizing background radiation (Haardt & Madau 2001) is turned on, ramping up to a constant value by  $z = z_{\text{UV}} - 1$

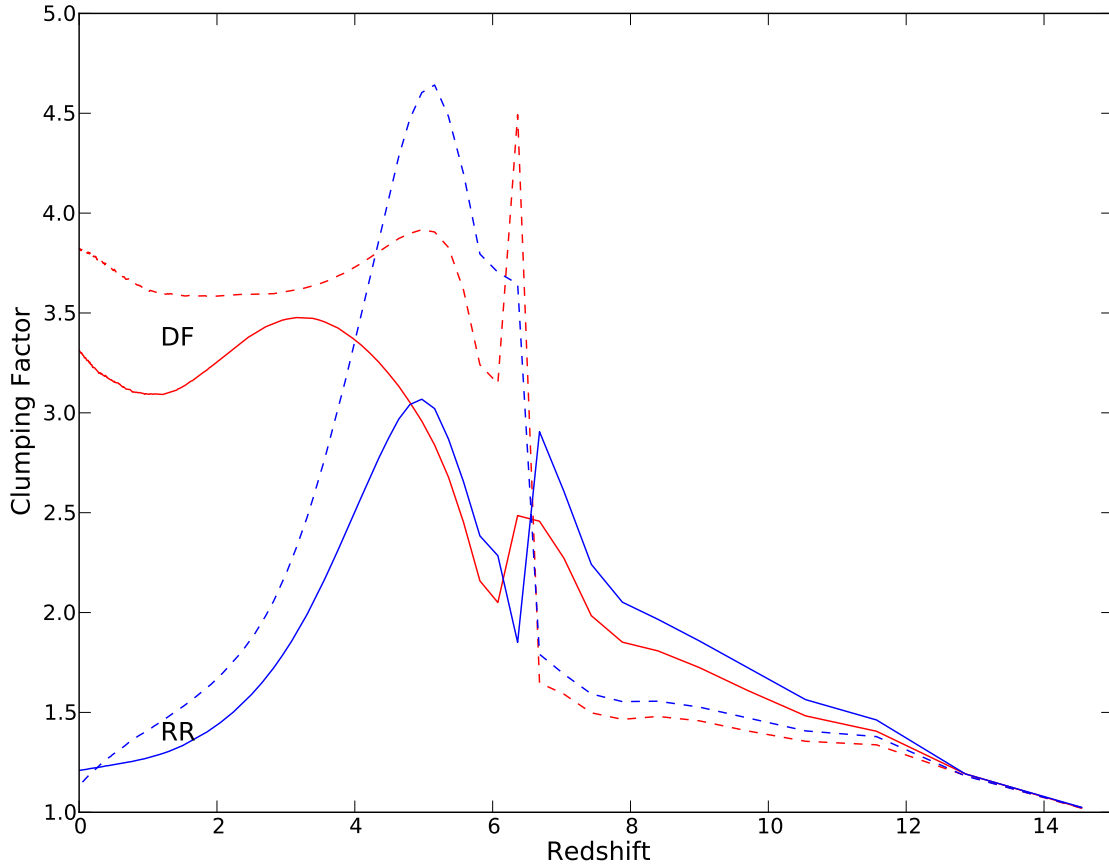


Fig. 1.— Comparison of two methods for calculating the clumping factor for simulation 50\_1024\_7 (UV background turned on at  $z = 7$ ) with different weights. Red lines: clumping calculated via density field (DF) method. Blue lines: clumping via recombination rate (RR) method (see Section 2.2). Solid lines correspond to weighting by volume, and dashed lines correspond to weighting by baryon overdensity. We believe the RR method, with volume weighting, is a more accurate measure of clumping.

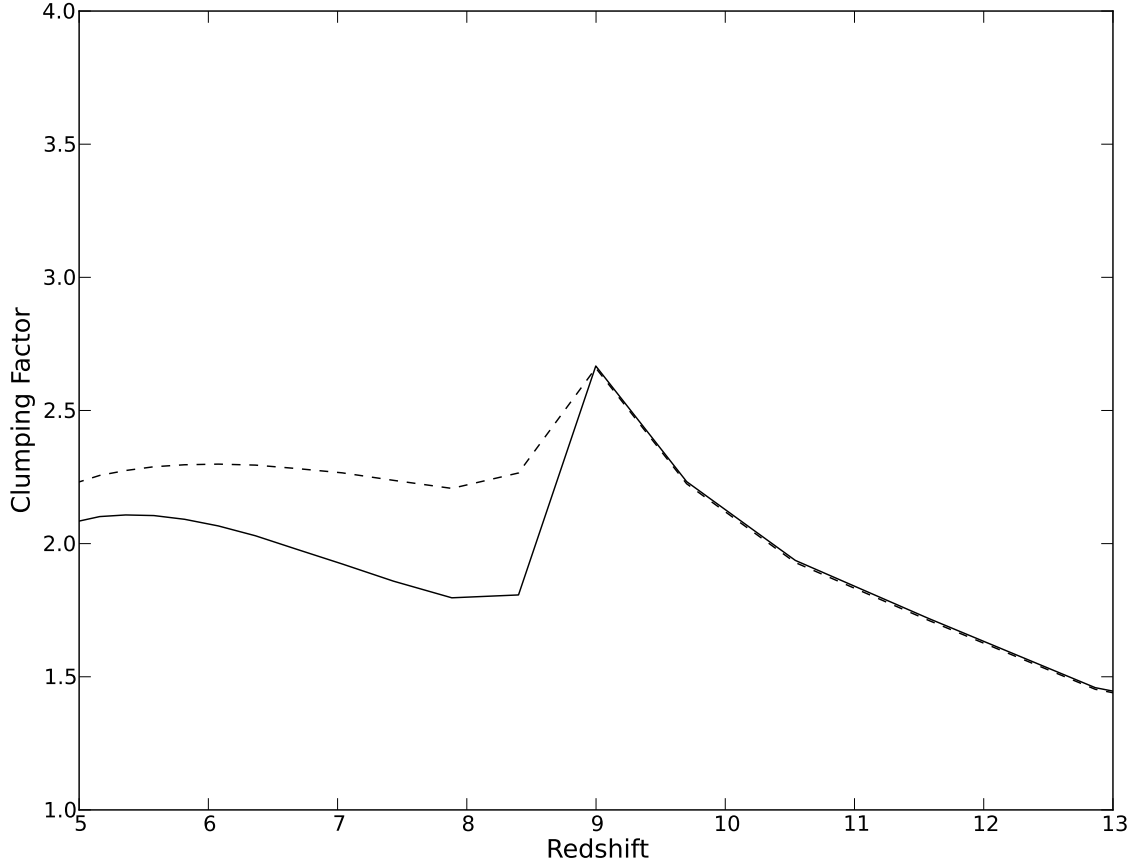


Fig. 2.— Effects of different “density cuts” on the clumping factor from our  $1536^3$  simulation, using the RR method in Equation (15). Solid line: clumping factor summed over cells with overdensity between  $1 < \Delta_b < 100$ , excluding low-density voids with  $\Delta_b < 1$ . Dashed line: including all cells with  $\Delta_b < 100$ .

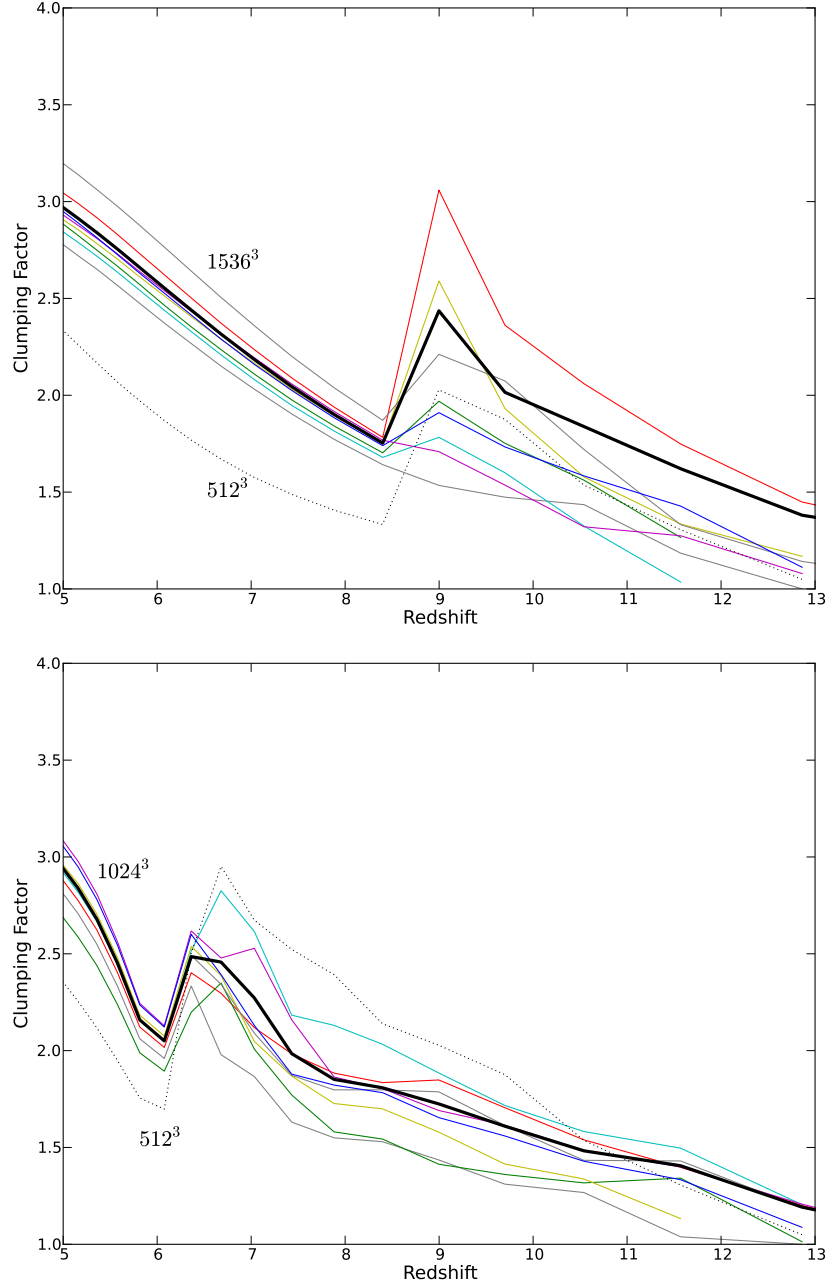


Fig. 3.— Comparison of convergence and cosmic variance among simulations. Values of  $C_H$  agree for  $1024^3$  and  $1536^3$  simulations, with variance computed over eight sub-volumes in our simulations. Top panel: eight  $768^3$  sub-volumes in  $1536^3$  run. Bottom panel: eight  $512^3$  sub-volumes in  $1024^3$  run. In each panel, our original  $512^3$  run is shown as dotted black line, and values for  $1536^3$  and  $1024^3$  runs as heavy black lines. Large variations in  $C_H$  at high redshifts arise from small numbers of cells prior to turn-on of the ionizing background at  $z = 9$  (top) and  $z = 7$  (bottom). For the  $1536^3$  simulation (top panel), the clumping factor is well-fitted by  $C_H(z) = (2.9)[(1+z)/6]^{-1.1}$  between  $5 < z < 9$ .

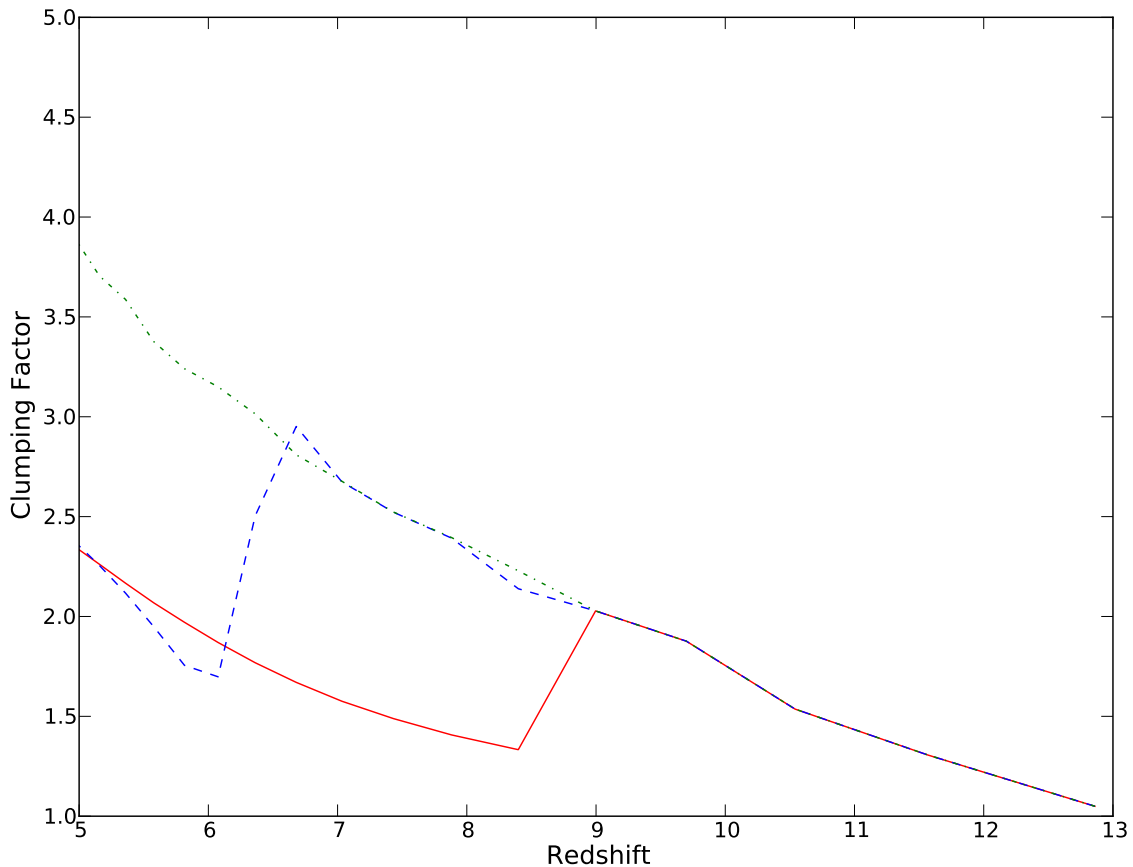


Fig. 4.— Clumping factor calculated via the density field (DF) method computed from three  $512^3$  IGM simulations, with sums weighted by volume (see eq. [14]). Red solid line has UV background (Haardt & Madau 2001) turned on at  $z = 9$  (simulation 50\_512\_9), blue dashed line at  $z = 7$  (simulation 50\_512\_7), and green dot-dashed line has no background (simulation 50\_512\_0). We observe two tracks for  $C_H(z)$ : a high-track for redshifts above turn-on of the UV background, and a lower track after turn-on. During most of the reionization epoch, from  $6 < z < 12$ ,  $C_H$  lies between 1.5 and 3.



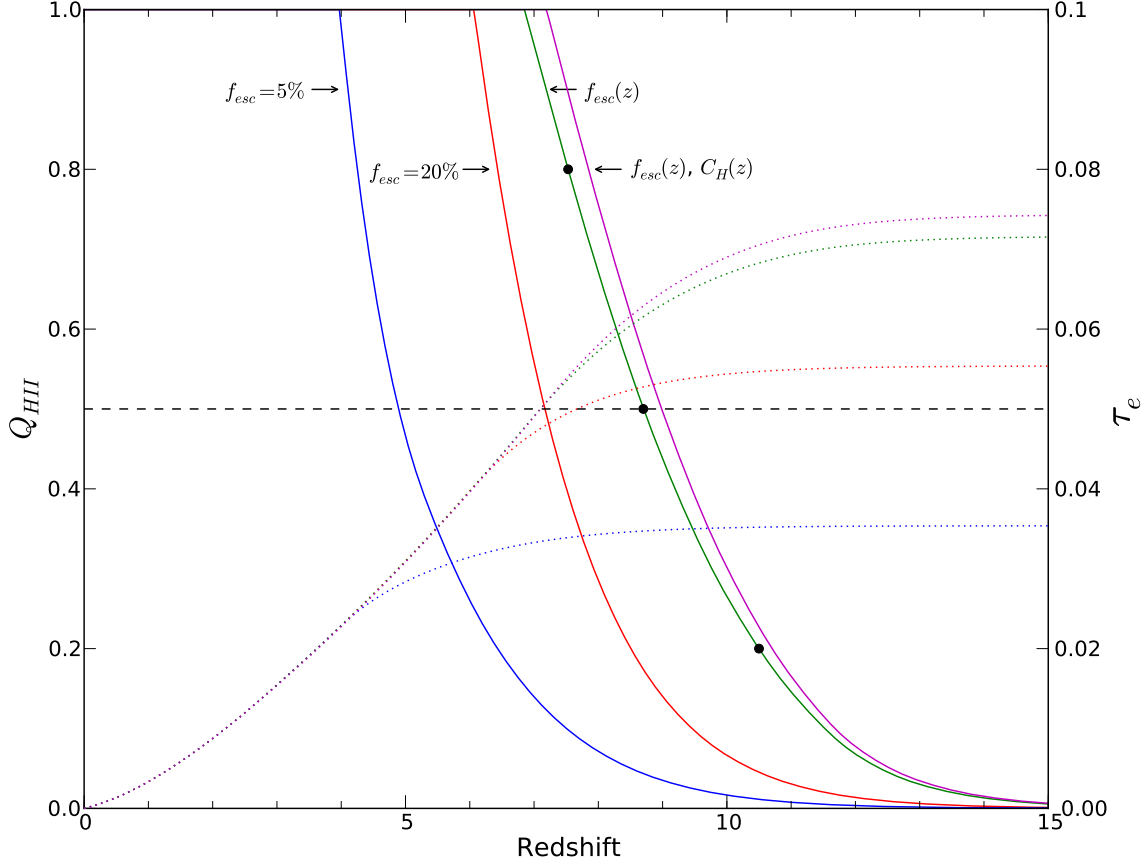


Fig. 5.— History of ionization fraction  $Q_{\text{HII}}(z)$  and CMB optical depth  $\tau_e(z)$  versus redshift (eqs. [3] and [17]) computed with  $T_e = 2 \times 10^4$  K,  $Q_{\text{LyC}} = 0.004$  ( $4 \times 10^{60}$  photons per  $M_\odot$ ) and using SFR history and evolving luminosity function from Trenti et al. (2010) integrated down to  $M_{\text{AB}} = -10$ . The IGM is assumed to be fully ionized when  $Q_{\text{HII}} = 1$ . Blue line: constant  $C_H = 3$  and  $f_{\text{esc}} = 0.05$  (this model reionizes too late to be viable). Red line: constant  $C_H = 3$  and  $f_{\text{esc}} = 0.2$ . Green line: constant  $C_H = 3$  but redshift-dependent  $f_{\text{esc}} = 1.8 \times 10^{-4}(1+z)^{3.4}$  (Haardt & Madau 2012). Magenta line: redshift-dependent  $C_H = 1 + 43z^{-1.71}$  (Pawlik et al. 2009) and  $f_{\text{esc}} = 1.8 \times 10^{-4}(1+z)^{3.4}$ . Our two preferred models with variable  $C_H$  or  $f_{\text{esc}}$  (green, magenta) naturally produce  $z_{\text{rei}} \approx 7$ . Solid black circles indicate redshifts of 20%, 50%, and 80% ionization; the duration  $\Delta z \approx 3$  is defined between 20% and 80% points.

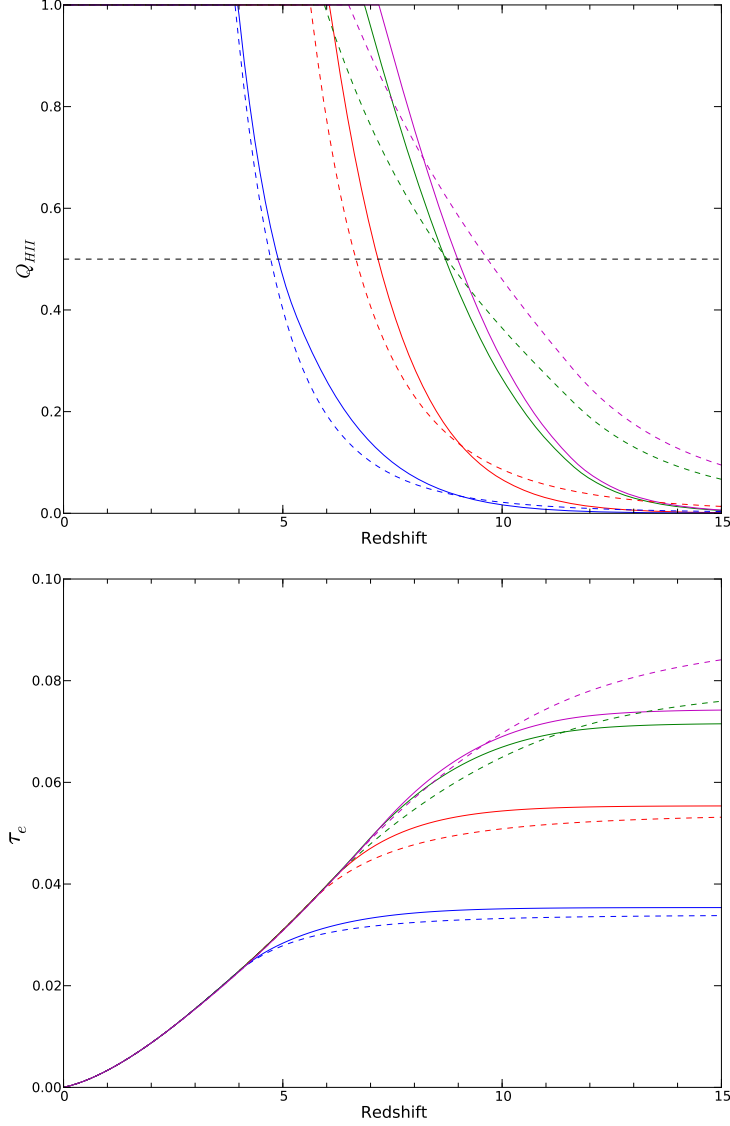


Fig. 6.— Top: Volume filling factors,  $Q_{\text{HII}}$ , with same color codes as Fig. 5, comparing two models for SFR history. Solid lines show SFR history from Trenti et al. (2010), and dashed lines show SFR from equation (53) in Haardt & Madau (2012), which is larger and more extended at higher redshifts, particularly for  $z > 8$ . Bottom: Corresponding CMB optical depths  $\tau_e(z)$ . Additional optical depth may arise from sources at  $z > 7$ .

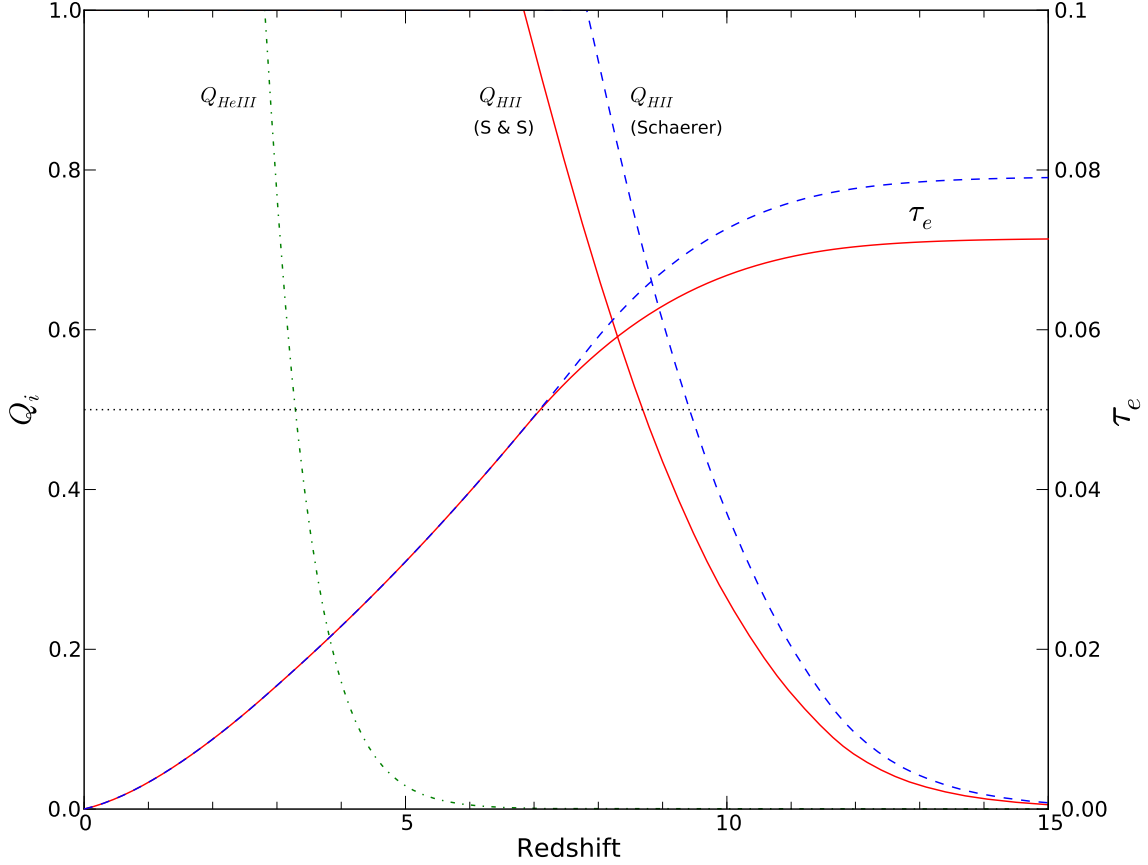


Fig. 7.— Example of the output for  $Q_{\text{HII}}(z)$ ,  $Q_{\text{HeIII}}(z)$ , and  $\tau_e(z)$  from our on-line SFR/reionization simulator. Solid lines show model atmospheres labeled as Sutherland & Shull (S&S), while dashed lines are for Schaerer (2002, 2003), assuming  $Z = 0.02Z_{\odot}$ . Models assume SFR history of Trenti et al. (2010) and parameters with constant  $C_H = 3$  and redshift-dependent  $f_{\text{esc}} = 1.8 \times 10^{-4}(1+z)^{3.4}$  (Haardt & Madau 2012). Dot-dashed line shows He III ionization history,  $Q_{\text{HeIII}}(z)$ , computed for QSO (4-ryd continuum) ionization as described in Section 3.3. In these models, H I is fully ionized by  $z \approx 7$  and He III by  $z \approx 2.7$ . Additional optical depth may arise from sources at  $z > 7$ .

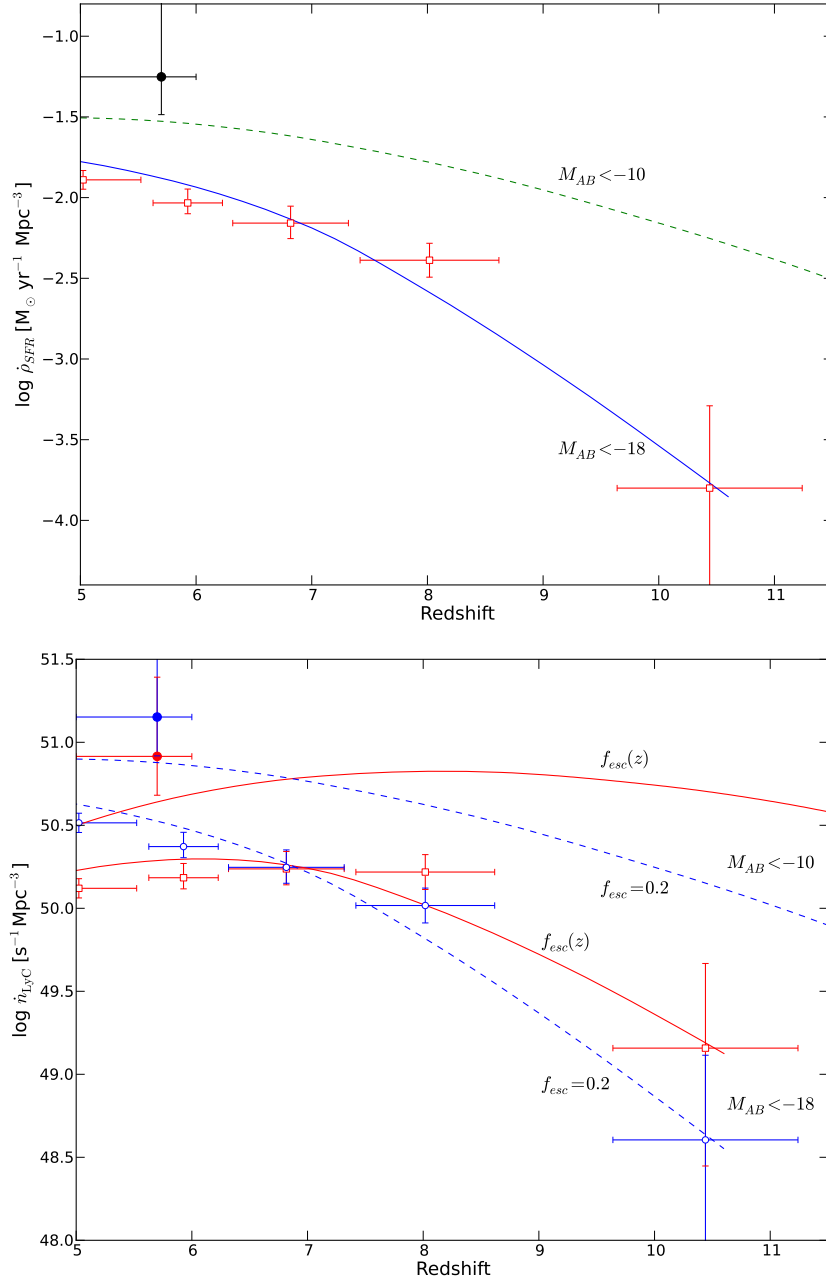


Fig. 8.— Top: Co-moving SFR density ( $\dot{\rho}_{\text{SFR}}$ ) from halo mass function model (Trenti et al. 2010) integrated for galaxies down to  $M_{\text{AB}} = -18$  (solid blue line) and to  $-10$  (dotted green line). Red data points are from Bouwens et al. (2011a) for galaxies down to  $M_{\text{AB}} = -18$ . Solid data point at  $z \approx 5.5$  is from ionizing background constraint (Eq. 21), using Haaradt & Madau (2012) model of  $\Gamma_H(z)$  and LyC mean free paths from (Songaila & Cowie 2010). Bottom: Co-moving emissivity,  $\dot{n}_{\text{LyC}}$ , of LyC photons, corresponding to above SFRs, integrated to  $M_{\text{AB}} = -18$  and  $-10$ . We use a LyC production parameter  $Q_{\text{LyC}} = 0.004$  ( $10^{53.1}$  LyC photons  $\text{s}^{-1}$  per  $M_{\odot} \text{yr}^{-1}$ ) and two different escape-fraction models:  $f_{\text{esc}} = 0.2$  (blue curves and data points) and  $f_{\text{esc}}(z) = (1.8 \times 10^{-4})(1+z)^{3.4}$  (red curves and data points).